International Journal of Heat and Mass Transfer 67 (2013) 944–954

Contents lists available at ScienceDirect

International Journal of Heat and Mass Transfer

journal homepage: www.elsevier.com/locate/ijhmt

Heat transfer in a high Hartmann number MHD duct flow with a circular cylinder placed near the heated side-wall

Wisam K. Hussam, Gregory J. Sheard *

Department of Mechanical and Aerospace Engineering, Monash University, VIC 3800, Australia

ARTICLE INFO

Article history:
Received 24 April 2013
Received in revised form 24 August 2013
Accepted 24 August 2013

Keywords:
MHD
Quasi 2D
Hartmann
Asymmetrical cylinder
Duct flow
Channel flow
Heat transfer enhancement

ABSTRACT

The heat transfer from the side-wall of a duct through which an electrically conducting fluid flows within a strong transverse magnetic field is investigated. A circular cylinder aligned with the magnetic field is offset from the duct centerline. In this configuration the flow is well described by a quasi-two-dimensional model and is therefore solved on a two-dimensional domain. The effects of blockage ratio, gap ratio and Reynolds number on the flow and heat transfer are considered. An optimal cylinder position is determined using an efficiency index defined as the ratio of heat transfer enhancement to pressure drop penalty resulting from insertion of the cylinder in the channel. Cylinder placement with gaps to the heated wall of between 0.83 and 1.4 diameters performed best, achieving at least 95% of the peak efficiency indices for each blockage ratio. These gap ratios corresponded to the periodic shedding of alternating-sign vortices into the wake which interacted with the heated side-wall boundary layer to form counter-rotating vortex pairs carrying hot fluid into the duct interior. By offsetting the cylinder from the wake centreline, heat transfer enhancement of up to 48% compared to the centreline placement is achieved with only a modest increase in the pressure head losses from cylinder drag.

1. Introduction

Magnetohydrodynamic (MHD) flow in rectangular ducts in the presence of a transverse magnetic field occur in metallurgical processing applications, and within the cooling blankets enveloping magnetic confinement fusion reactors. Under a sufficiently strong magnetic field, the electrically conducting fluid interacts with the applied magnetic field in such a way that disturbances parallel to the magnetic field are strongly suppressed, giving vortices a propensity to elongate and align parallel with the magnetic field [1,2]. Hence these MHD duct flows typically comprise a two-dimensional core flow confined by boundary layers on the duct walls. The duct walls perpendicular to the magnetic field contain boundary layers known as Hartmann layers, which exert a friction on the interior two-dimensional flow, leading to the development of quasi-two-dimensional models for these flows [1,3]. Friction from the Hartmann layers acts to dampen turbulent structures in the flow. Considering heat-intensive applications such as in magnetic confinement fusion reactor blankets, this damping works against the desire to maximise turbulent mixing and convective heat transfer in the cooling blanket ducts (where a large amount of heat must be removed [4]). This has promoted numerous investigations into the stability and turbulent transition in MHD duct flows [5–7], including the use of conducting wall segments or inclusions [8,9], magentic field 'obstacles' [10,11]. For a review of liquid–metal flows in magnetic confinement fusion reactor blankets, see [12].

In addition to liquid–metal cooling systems in fusion reactors, other liquid–metal duct flow applications include the cooling of nuclear fission reactors and high-performance computing infrastructure. Beyond MHD applications, channel flows exhibiting quasi-two-dimensional characteristics appear in applications ranging from microfluidics through to geophysical flows.

In this study we restrict our consideration to the scenario where the duct is heated through one side-wall, which is perpendicular to the quasi-two-dimensional plane. In the absence of turbulence and disregarding natural convection effects, the side-wall boundary layers, known as Shercliff layers, are laminar, and the mode of heat transfer is via conduction. In fact, the Shercliff layers do develop a three-dimensional instability [13], but their quasi-two-dimensional approximation under the model employed in this work has been shown to exhibit the same thickness scaling with Hartmann number, and similar turbulent, friction and some stability properties [3,5,14–16]. Recent three-dimensional simulations [17] at a Reynolds number of 10^5 lend further support to these observations at higher Hartmann numbers (greater than $O(300)$), with the caveat that channel turbulence disrupted the otherwise thin Hartmann and Shercliff layers. [17] found that the Shercliff layers laminarized at a Hartmann number of 400. By comparison,

* Corresponding author. Tel.: +61 3 9905 1182.
E-mail address: Greg.Sheard@monash.edu (G.J. Sheard).

0017-9310/$ - see front matter © 2013 Elsevier Ltd. All rights reserved.
http://dx.doi.org/10.1016/j.ijheatmasstransfer.2013.08.081

Nomenclature

a	duct depth (out of plane)
B	uniform magnetic field strength
C_D	cylinder drag coefficient (x-direction)
C_L	cylinder lift coefficient (transverse y-direction)
d	cylinder diameter
f	wake oscillation frequency
F'_d	cylinder drag force per unit span
F'_l	cylinder lift force per unit span
F	Fourier transform
G	gap between cylinder and heated duct side-wall
H_d	Hartmann friction parameter
Ha	Hartmann number
HI	heat transfer increment
HI_{asym}	HI comparing offset and centerline cylinder placement
HR	heat transfer enhancement ratio
L	duct half-width (in the y-direction)
L_{duct}	length of duct section
n	number of out-of-plane duct walls (here $n = 2$)
Nu	time-averaged Nusselt number
Nu_0	Nu for the same duct without a cylinder
Nu_{asym}	same as Nu
Nu_{sym}	Nu but with cylinder positioned on duct centreline
Nu_{w}	local Nusselt number along heated side-wall
p	kinematic pressure
Pe	Peclet number
Pr	Prandtl number
PR	pressure penalty ratio
Ra	Rayleigh number
Re	Reynolds number (based on L)
Re_d	Reynolds number (based on d)
Re_m	magnetic Reynolds number
St	Strouhal number
t	time
T	temperature scalar
T_f	bulk fluid temperature
T_o	cold wall and fluid temperature
T_w	hot wall temperature
$\mathbf{u}$	quasi-two-dimensional velocity vector
U_0	peak fluid velocity at duct inlet
x	Cartesian coordinate (streamwise direction)
y	Cartesian coordinate (transverse direction)
z	Cartesian coordinate (vertical out-of-plane direction)

Greek symbols

β	blockage ratio
γ	position ratio
δ_s	Shercliff layer thickness (on duct side-walls)
ΔP	total pressure drop in duct
ΔP_0	duct pressure drop (no cylinder)
ΔP_{cyl}	contribution of cylinder to pressure drop penalty
Δt	time step size (numerical time integration)
ΔT	reference temperature difference, $T_w - T_o$
η_{eff}	efficiency index
κ_T	fluid thermal diffusivity
ν	fluid kinematic viscosity
ρ	fluid density
σ	magnetic permeability of the fluid
ω	vorticity (quasi-two-dimensional plane)

[18] used a Large Eddy Simulation to demonstrate that at a Reynolds number of 14 500 turbulence was localized in the Shercliff layers at Hartmann numbers of 43.5 and 58, but that these became fully laminar at a Hartmann number of 65.25. Hence a picture emerges whereby even at high Reynolds numbers, the magnetohydrodynamic damping effects can laminarize the flow to a state that is well-described by a quasi-two-dimensional model, provided that the Hartmann numbers are sufficiently high.

Under the conditions where the quasi-two-dimensional model describes the physical duct flow, turbulence promoters become an attractive option for generating flow disturbances necessary to invoke convective heat transfer along the heated duct side-wall. Due to the quasi-two-dimensional flow behaviour, a prototypical turbulence promoter can be represented by a cylindrical obstacle aligned with its span parallel to the magnetic field. Such a configuration has motivated study into the effect of a magnetic field on disturbances in the wake of a cylinder [8,19,20]. Experiments [14] and numerical [21–23] investigations have considered the confinement of a cylinder within a duct exposed to a transverse magnetic field. For the case with electrically insulated duct walls, [23,24] demonstrated that the heat transfer rate under a strong transverse magnetic field could be improved by more than a factor of two over the laminar flow with an increase in the pressure drop along the duct. More recently, [25] employed a transient growth analysis determining that the instability leading to vortex shedding behind a cylinder in such a magnetohydrodynamic duct flow can be optimally perturbed by disturbing the flow very near to the cylinder. This motivated a subsequent numerical investigation whereby a torsional oscillation was imparted on a cylinder located within a quasi-two-dimensional duct flow [26] to promote vortex shedding and to enhance heat transfer.

These studies typically considered cylinder placement on the duct centreline, leading to the observation of a tradeoff between the desire for a cylinder sufficiently large to produce wake vortices that interact with the heated Shercliff layer and increase heat transfer, and the desire for a low blockage ratio to minimise the pressure drop penalty in the duct flow. A natural development of this concept is to employ a smaller cylinder positioned closer to the heated side-wall. It is therefore pertinent to review investigations into the placement of a cylinder near to a plane wall.

This problem has received attention for non-magnetohydrodynamic flows through its applications in ground effect and biological flows. Studies across a wide range of Reynolds numbers [27–32] have consistently demonstrated the existence of a critical gap ratio between cylinder and wall, below which vortex shedding is suppressed. Numerical simulations [30] demonstrated that the critical gap ratio $(G/d)_{\text{crit}}$ below which shedding is suppressed was infinite for Reynolds numbers below the critical Reynolds number for vortex shedding in open flow, and with increasing Reynolds number up to 600, the critical gap ratio decreased towards a value of 0.2 which was preserved at higher gap ratios. Experiments over Reynolds numbers $1.2 \times 10^3 \leqslant Re_d \leqslant 4.96 \times 10^3$ [31] find a regime of vortex pairing for gap ratios $0.25 \leqslant G/d \leqslant 0.375$ with vortex shedding above $G/d = 0.375$. For $Re_d = 1.89 \times 10^4$, [32] detected three-dimensional flow for $G/d \gtrsim 0.7$, two-dimensional vortex shedding over $0.53 \leqslant G/d \lesssim 0.7$, and intermittent shedding below $G/d \approx 0.5$. An experiment by [28] at the nearby Reynolds number $Re_d = 2.2 \times 10^4$ suggest a lower bound on the intermittent shedding regime of $G/d = 0.25$. Finally, [27] also first detected vortex shedding above $G/d = 0.3$ at the higher Reynolds number $Re_d = 4.5 \times 10^4$, and further found that above the critical gap ratio, the shedding frequency remained nearly constant.

It has been established that the interaction of wake vortices with a boundary layer adjacent to a heated wall enhances heat transfer through the wall [23,26]. Considering the limits of the gap between cylinder and wall we have two scenarios: at the limit of small gap ratio, the suppression of vortex shedding will lead to a decrease in heat transfer, and as the gap ratio becomes large, heat transfer again will decrease as the wake vortices move far away from the heated wall. It is therefore expected that some finite gap ratio exists maximising the rate of heat transfer. This study aims to establish the relationship between duct blockage ratio, gap ratio and heat transfer for quasi-two-dimensional magnetohydrodynam-ic duct flow.

The paper is organised as follows. The problem is defined in Section 2, which also presents the governing equations and parameters. The methodology is presented in Section 3, which describes the numerical method, model setup, boundary conditions and validation. Results and discussion follow in Section 4, with conclusions drawn in Section 5.

2. Problem definition

The geometry of the problem under consideration is shown in Fig. 1. A long duct has a uniform rectangular cross-section with width $2L$ and an out-of-plane height a, carrying an electrically conducting fluid. A strong uniform magnetic field acts perpendicular to the x-y plane, and a circular cylinder with diameter d is placed in the duct with its axis parallel to the magnetic field a distance G from a heated side-wall. The blockage ratio $\beta = d/(2L)$ characterises the occlusion of the duct by the cylinder. The cylinder position can be defined relative to the distance to the channel centreline [33] as $\gamma = G/(L - d/2)$. The value of γ varies between 1 when the cylinder is placed symmetrically between the side-walls to 0 when it is in contact with the heated side-wall. It is also sensible to characterize the cylinder proximity to the heated wall, given that the interaction between the cylinder wake and the heated wall is expected to provide the primary heat transfer mechanism. Therefore results will also be considered in terms of the gap ratio G/d. Table 1 summarizes the gap ratios G/d considered in this study for different blockage and position ratios.

The duct walls and the cylinder are assumed to be electrically insulated, and a homogeneous magnetic field with a strength B is imposed parallel to the cylinder axis. As described in Sommeria and Moreau [1], for a high Hartmann number, the magnetic Reynolds number Re_m, which represents the ratio between the induced and the applied magnetic field is very small. Thus, the induced magnetic field is negligible and the resulting magnetic field is maintained in the z-direction only. Depending on the orientation of the channel, natural convection may emerge as the dominant heat transfer mechanism under certain conditions [22,34], though this effect is not considered in the present study. Barleon et al. [35] provide guidance with respect to the effect of natural convection. They demonstrate that for MHD flow in a vertically aligned duct, at Hartmann numbers $Ha \gtrsim 400$ (such as those considered in this study), natural convection is negligible for Rayleigh numbers less than $Ra \approx 10^4$, while $Ra \gtrsim 10^4$, the Nusselt number associated with natural convection remained consistently less than that for an equivalent channel without a magnetic field.

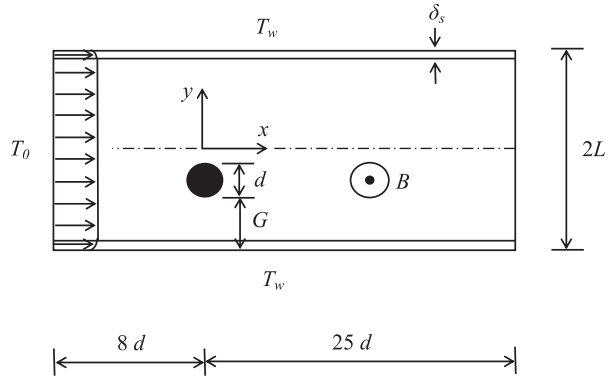

Fig. 1. Schematic representation of the system under investigation. The magnetic field B acts in the out-of-plane direction, parallel to the cylinder axis. δ_S is the thickness of the Shercliff layer, $2L$ is the duct width, and and d is the cylinder diameter, respectively. The blockage ratio is $\beta = d/(2L)$, the position ratio is $\gamma = G/(L - d/2)$, and the gap ratio is G/d.

Table 1
The relationship between gap ratio G/d and position ratio γ at the different blockage ratios considered in this study.

γ	G/d for $\beta = 0.1$	0.2	0.3	0.4
1	4.5	2.0	1.15	0.75
0.5	2.25	1.0	0.58	0.38
0.25	1.13	0.5	0.29	0.19

2.1. Governing equations and parameters

Under these conditions the flow is quasi-two-dimensional and consists of a core region, where the velocity is invariant along the direction of the magnetic field, and a thin Hartmann layer at the wall perpendicular to the magnetic field. The quasi-two-dimensional model was derived by Sommeria and Moreau [1] by averaging the flow quantities along the magnetic field direction. A thorough description of this model is given in [3,15]. Here lengths are scaled by the cylinder diameter d, pressure by ρU_0^2, where ρ is the density and U_0 is the peak inlet velocity, time by d/U_0, and temperature by the imposed temperature difference between the duct side-walls, ΔT [34,36].

This produces dimensionless magnetohydrodynam-ic equations governing continuity, momentum, and energy expressed as

$$\nabla \cdot \mathbf{u} = 0, \tag{1}$$

$$\frac{\partial \mathbf{u}}{\partial t} + (\mathbf{u} \cdot \nabla)\mathbf{u} + \nabla p = \frac{1}{Re_d}\nabla^2 \mathbf{u} - \frac{H_d}{Re_d}\mathbf{u}, \tag{2}$$

$$\frac{\partial T}{\partial t} + (\mathbf{u} \cdot \nabla)T = \frac{1}{Pe}\nabla^2 T, \tag{3}$$

where $\mathbf{u}$, p and T are, respectively, the velocity, pressure, and temperature fields, projected onto the x-y plane, and t is time. It is noted that the energy equation is sometimes written to include terms describing the effects of viscous dissipation and Joule heating (e.g., see [37]), though here these effects are not considered (following [34,38] and others), as their contributions are negligible for the application considered in this study [23].

The Reynolds number characterizes the ratio of inertial to viscous forces, and is defined as

$$Re_d = U_0 d/\nu, \tag{4}$$

where ν is the fluid kinematic viscosity. The Hartmann friction parameter is defined as

$$H_d = n\left(\frac{d}{a}\right)^2 Ha, \tag{5}$$

where n is the number of Hartmann layers in the flow (here $n = 2$ due to the out-of-plane duct walls running parallel to the x–y plane). The Hartmann number characterizes the square root of the ratio of electromagnetic to viscous forces, and is defined as

$$Ha = aB\sqrt{\frac{\sigma}{\rho\nu}}, \tag{6}$$

where σ and B are the magnetic permeability of the fluid and the applied magnetic field strength, respectively. Finally, the Peclet number characterizes the ratio of the rate of advection to the rate of diffusion of the temperature field, and is defined as $Pe = Re_d Pr$. The Prandtl number $Pr = \nu/\kappa_T$, where κ_T is the thermal diffusivity of the fluid, characterizes the ratio of viscous to thermal diffusion in the fluid.

This study investigates the fluid structure and heat transfer of MHD flow past a circular cylinder positioned various distances from a heated side-wall in a rectangular duct in the presence of a strong uniform magnetic field. Blockage ratios $0.1 \leqslant \beta \leqslant 0.4$ and Reynolds numbers ($100 \leqslant Re_d \leqslant 3000$) are considered for a constant Hartmann friction parameter. A Prandtl number $Pr = 0.022$ is used throughout, representative of the eutectic alloy GaInSn.

A constant Hartmann friction parameter $H_d = 100$ is employed throughout this study. The validity of the quasi-two-dimensional model is dependent on criteria relating to combinations of the Hartmann number Ha and the Reynolds number Re. In order for the Hartmann layers to remain laminar, and therefore adopt the exponential profile required by the model, experiments by [39] showed that the condition $Re/Ha \lesssim 150$ to 250 had to be satisfied. Recasting H_d in terms of Hartmann number and using the blockage ratio definition to eliminate d gives

$$Ha = \frac{1}{8}\frac{a^2}{L^2\beta^2}H_d, \tag{7}$$

while Re relates to Re_d through $Re/Re_d = L/d = 1/(2\beta)$. Combining these gives

$$Re/Ha = 4\beta\frac{L^2}{a^2}\frac{Re_d}{H_d}. \tag{8}$$

Hence for the present simulations at $Re_d = 2000$ and 3000 and $\beta = 0.1$ to 0.4, $(Re/Ha)(a^2/L^2)$ ranges from 8 to 48. Provided $a/L \lesssim 2$, this condition is satisfied.

Three-dimensional results from [40] suggested that flow in a duct with a square cross-section was quasi-two-dimensional for $Ha \geqslant 200$. For $H_d = 100$, we have $Ha(L^2/a^2) = 1250$ and 313 at $\beta = 0.1$ and 0.2, falling to 139 and 78.1 at $\beta = 0.3$ and 0.4. Hence some quantitative discrepancy would be expected between our computed quasi-two-dimensional results at higher blockage ratios and a corresponding physical flow. This is further supported by the recent computations of [41], which demonstrate that even up to interaction parameters $N = Ha^2/Re \approx 16$ discrepancies exist between the quasi-two-dimensional model and the three-dimensional flow. They observed that up to $N \approx 16$ the quasi-two-dimensional model overestimates the energy retained in primary wake vortices, leading to a more irregular vortex shedding than is seen in the three-dimensional flow. However, they also expected that the quasi-two-dimensional approximation would improve at higher N as larger scales also become damped by the stronger magnetic fields. The interaction parameter can be written in terms of Re_d and H_d as

$$N\frac{L^2}{a^2} = \frac{1}{32\beta^3}\frac{{H_d}^2}{Re_d}. \tag{9}$$

For $Re_d = 2000$ and $H_d = 100$ this yields $N(L^2/a^2) \approx 156$ and 19.5 for $\beta = 0.1$ and 0.2, while for $\beta = 0.3$ and 0.4, $N(L^2/a^2) \approx 5.8$ and 2.4 are obtained, respectively. Again, strong performance of the quasi-two-dimensional model can be expected under the conditions described in this paper at smaller blockage ratios.

While the problem under investigation is motivated by flow and heat transfer within the cooling blankets of magnetic confinement fusion reactors, the quasi-two-dimensional model we employ modifies the two-dimensional Navier–Stokes equations only through the addition of a linear friction term in the momentum equation, and therefore invokes far broader fundamental interest with applications ranging from quasi-two-dimensional turbulence [16] to geophysical flows.

3. Numerical methodology

3.1. Spectral element solver and computational model

A nodal spectral-element method is utilized to discretise the governing flow and energy equations in space, and a third-order scheme based on backwards differentiation is employed for time integration [42]. The setup of the system is the same as that described in Hussam et al. [23]. The cylinder is located at $8d$ and $25d$ from the inlet and outlet, respectively, which was found to be sufficient to obtain domain independent results following a care full domain dependence study. The computational domain is divided into a grid of elements. Elements are concentrated in the vicinity of the cylinder and the heated wall to capture the small-scale structures in the flow. The meshes comprise between 1196 and 2391 elements, depending on blockage and gap ratios. Here, the asymmetrically positioned cylinder requires the creation of new meshes, and thus further grid-independence tests are performed to ensure that adequate spatial resolution is maintained for the simulations described in this study.

3.2. Boundary conditions

The boundary conditions imposed on Eqs. (1)–(3) are as follows: A no-slip boundary condition for velocity is imposed on all solid walls. At the channel inlet, the analytical solution to Eqs. (1) and (2) for fully developed quasi-two-dimensional flow through the channel considered in this study without any obstacle is applied [16,22]. At the exit, we impose a Dirichlet condition for a constant reference pressure, and a Neumann condition for a zero outward-normal gradient on the velocity field. This is a conventional outflow boundary condition for incompressible spectral-element flow simulations [43–45]. A high-order Neumann condition for the pressure gradient is imposed on the Dirichlet velocity boundaries to preserve the third-order time accuracy of the scheme [42]. The temperature of the incoming stream and the unheated side-wall is specified as T_o, and at the heated side-wall as T_w (note that $T_w - T_o = \Delta T$. The cylinder is thermally insulated (i.e. a zero normal temperature gradient is imposed at its surface).

3.3. Validation and grid independence

This study employs meshes with the same h-resolution (element distribution and refinement) and the same quasi-two-dimensional model as were validated in [23,25,26], and those papers should be consulted for further details. Here an additional study was performed to determine the element polynomial order that is required to produce results accurate to within a threshold level of 0.3%, given that new meshes for constructed to model the placement of the cylinder at various distances from the heated side-wall. The parameters monitored to test for convergence included a Strouhal number characterizing the wake oscillation frequency f, defined as

$$St = \frac{fd}{U_0} \tag{10}$$

and a drag coefficient

$$C_D = \frac{F_d'}{\frac{1}{2}\rho U_0^2 d}, \tag{11}$$

where F'_d is the drag force per unit span exerted by the fluid on the cylinder.

The element polynomial degree was varied between 4 and 9, while keeping the macro-element distribution unchanged. Convergence tests were performed on two cases, chosen at the upper end of the parameter range of this study. The first case had $\beta = 0.1$, $Re_d = 3000$, $H_d = 100$ and $\gamma = 0.25$, while the second case had $\beta = 0.4$, $Re_d = 3000$, $H_d = 100$ and $\gamma = 0.25$. The desired error threshold was found to be met using elements with a polynomial degree of 7, which is used hereafter.

The formulation was also tested to ensure that the solution was independent of the time step size, Δt. Halving the time step from 0.001 to 0.0005 for the aforementioned test cases produced negligible variation in St and C_D, reflecting the third-order time accuracy and tight stability constraints of the scheme [42,43].

4. Results and discussion

4.1. Flow structures and temperature field

When a cylinder is offset from the centreline of a duct, the dynamics of the flow differ due to the presence of the fixed wall closer to the cylinder surface. A Reynolds number of 2000 and Hartmann number $H_d = 100$ have been chosen to demonstrate the interaction of the wall boundary layers parallel to the magnetic field and that of the cylinder. Figs. 2 and 3 illustrate the effect of the blockage ratio β and gap ratio γ on vortex shedding from the cylinder for these parameters. Plots of the logarithm of the magnitude of vorticity (where vorticity $\omega = \nabla \times \mathbf{u} = \partial v/\partial x - \partial u/\partial y$ for a two-dimensional velocity field) are presented to reveal the both the vortical structure and any wake-side wall interactions in the flow. While this quantity obscures the sign of the vorticity field, this is often apparent from the geometry. Importantly, the logarithmic nature of this quantity elucidates details in the flow that are difficult to detect in a direct plot of vorticity due to the strong Hartmann damping in these flows. For $\beta = 0.1$, when the cylinder is symmetrically in the plane channel (i.e. $\gamma = 1$), a wake comprising two well-defined rows of vortices is formed with clockwise negative and counter-clockwise positive vortices shed from the top and the bottom separating shear layers behind the cylinder, respectively. When $\gamma = 0.5$, the wake behind the cylinder still displays a two-row vortex street convecting the extent of the downstream domain. At this position ratio, the nearer side-wall Shercliff layer is still a distance cylinder from the lower shear layer on the cylinder surface, and interacts only weakly with the wake region. As γ is decreased to 0.25 (a gap ratio of $G/d = 1.13$), a negative-signed vorticity entrained from the wall boundary layer downstream of the cylinder. This vorticity interacts with the negative-signed vortices shed from the upper shear layer on the cylinder. This results in the Kármán vortex street aligning into a single row of vortices.

For $\beta = 0.2$ and $\gamma = 1$ (not shown), the structure of the vorticity field was found to resemble that of $\beta = 0.1$ at $\gamma = 1$, though lower-wall shear layer was seen to interact weakly with the negative shear layer on the cylinder surface. At $\beta = 0.2$, the detachment of the wall shear layer at the cylinder location increased more significantly as the gap ratio decreased from 1 to 0.5, more than was observed at $\beta = 0.1$. As a consequence, the lower shear layer on the cylinder interacts strongly with the wall shear layer.

For $\beta \geqslant 0.3$ at $\gamma = 1$ (not shown), the wall shear layers interact significantly with the Kármán vortex street causing the wake vortices to decay much more quickly. For $\gamma \geqslant 0.5$, the boundary layer along the lower side of the cylinder and the shear layer along the wall effectively merge and roll up together before travelling further downstream. At the smallest position ratio of $\gamma = 0.25$ for $\beta = 0.4$ (Fig. 3), the wake vorticity on the upper side of the cylinder is stretched out as the wake advects downstream. For all $\gamma \leqslant 1$, there is a strong interaction between the wake vortices and the Shercliff layers. So much so that for $\gamma \leqslant 0.5$, the coherence of Kármán vortex street is completely lost.

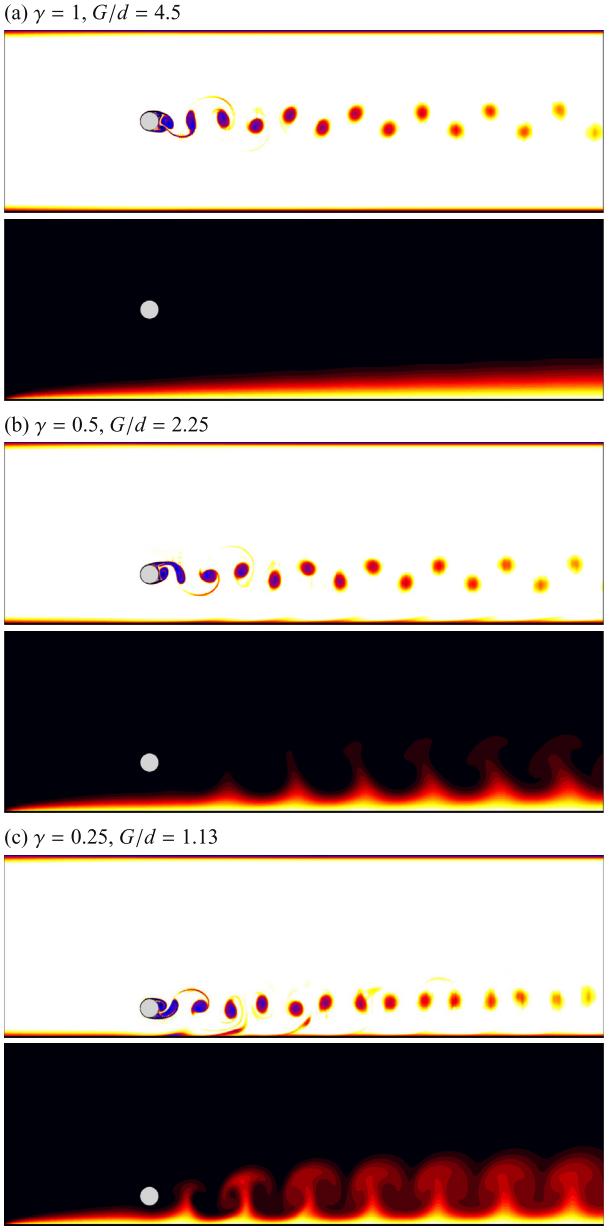

Fig. 2. Pairs of contour plots of $\log|\omega|$ (above) and temperature (below) for $H_d = 100$, $Re_d = 2000$ and β of 0.1 for gap ratios (a–c) of γ = 1, 0.5 and 0.25, respectively. For the logarithm of the absolute value of vorticity plots, levels are plotted over $-1 \leqslant \log|\omega| \leqslant 3$, with darker contours corresponding to regions of stronger vorticity. For the temperature plots, dark and light contours correspond, respectively, to colder and hotter regions, with contours plotted over $T_o \leqslant T \leqslant T_w$.

Summarizing our observations across the range of blockage ratios it is seen that for $G/d \approx 2 - 2.25$ at small blockage ratios ($\beta = 0.1$ and 0.2, e.g. Fig. 2b), the wake behind the cylinder is characterized by a two-row vortex street extending throughout the entire downstream. The wall boundary layer that develops along the surface parallel to the magnetic field at the cylinder location are far from the lower shear layer on the cylinder surface. On the other hand, for $G/d \approx 0.75$–1.15 at $\beta = 0.1$, 0.2 and 0.3 (e.g. Fig. 2c), the structure of the wake behind the cylinder is almost the same, while the wall

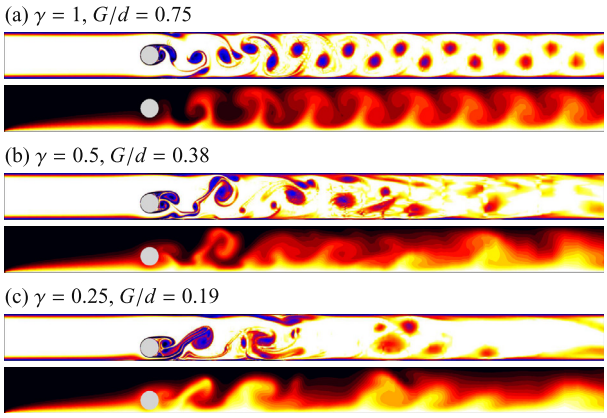

Fig. 3. Pairs of contour plots of $\log|\omega|$ (above) and temperature (below) for $H_d = 100$, $Re_d = 2000$ and β of 0.4 for gap ratios (a–c) of γ = 1, 0.5 and 0.25, respectively. Contour shading is as per Fig. 2.

boundary layer expands and separates from the wall downstream of the cylinder to form negative-sign vortex structures. For $G/d \approx 0.5 - 0.58$ at $\beta = 0.2$ and 0.3, the vortex street interacts strongly with the near-wall boundary layer, before deflecting away from the wall and into the duct interior.

In order to illustrate the importance of G/d characterizing the flow in the vicinity of the heated wall, a series of simulations were performed at a constant gap ratio $G/d = 0.75$ and a range of blockage ratios. The results are shown in Fig. 4. Across these blockage ratios, there is consistently a strong interaction between the heated wall and the cylinder wake within approximately $4d$ downstream, visible in both the vorticity and temperature field plots. For blockage ratio $\beta \leqslant 0.2$, the vortex street then deflects away from the heated wall. This is driven by pairing of wake vortices which then self-propel away from the hot wall. For $\beta = 0.2$ (far downstream) and 0.3 (in the near wake), a strong interaction between the wake and the Shercliff layer on the upper cold wall is observe. Due to the equal proximity of the side walls, for $\beta = 0.4$ the vortex street comprises regular vortices shed from the cylinder, entraining vorticity from both sides into the wake.

In order to better characterize the effect of vortex patterns on the wall heat transfer, instantaneous temperature plots accompany the vorticity plots in contours for different blockage ratios for gap ratios is also presented in Figs. 2–4. It will be show later that for blockage ratio $\beta = 0.1$, as the gap ratio decreases, the heat transfer increases markedly. This is due to the sweeping of the hot surface by the wake vortices, which transports low-temperature fluid towards the lower wall of the channel while the high-temperature fluid from thermal boundary layer is convected away to mix with the low-temperature fluid. In contrast, for $\beta = 0.4$, as the gap ratio is decreased to $\gamma = 0.25$, the unsteadiness in the flow is reduced significantly. This increases the thickness of the thermal boundary layer, and hence reduces the wall-normal temperature gradient along the hot wall and the associated heat transfer.

4.2. Fluctuating lift coefficient

The loss of periodicity and wake coherence seen at $\beta = 0.4$ at small gap ratios is undesirable from the perspective of enhancing heat transfer. To help quantify this effect, we consider the time history of the lift coefficient of the cylinder. The lift coefficient is defined as

$$C_L = \frac{F_l'}{\frac{1}{2}\rho U_0^2 d} \tag{12}$$

where F_l' is the lift force exerted by the fluid per unit span of the cylinder.

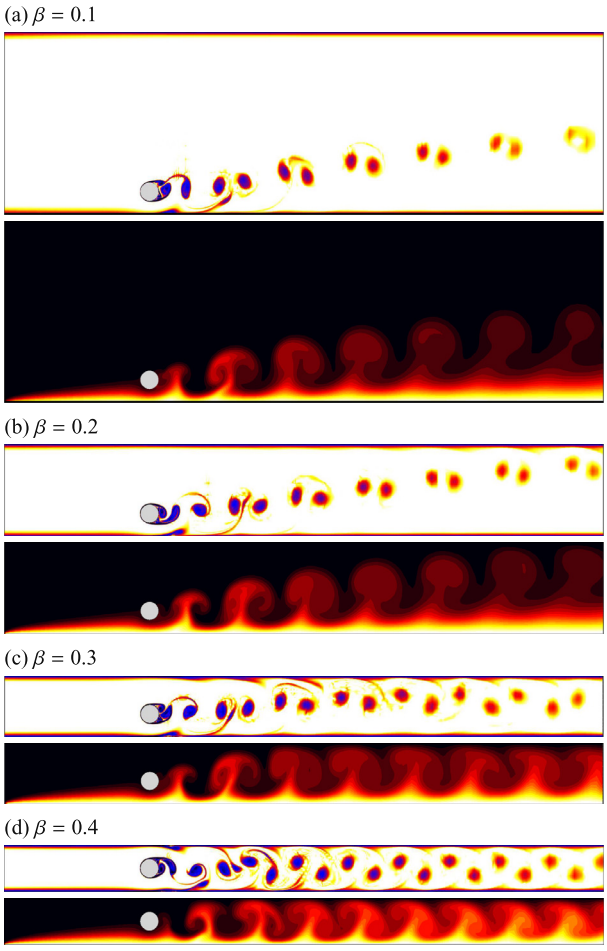

Fig. 4. Pairs of contour plots of $\log|\omega|$ (above) and temperature (below) for $H_d = 100$, $Re_d = 2000$ and $G/d = 0.75$ for blockage ratios as indicated. Contour shading is as per Fig. 2.

Fig. 5 presents the time history of the lift coefficient at different gap ratios for $Re_d = 2000$, $H_d z = 100$ and blockage ratios of 0.1 and 0.4. It can be seen that at the small blockage ratio $\beta = 0.1$ for all position ratios tested, the signal is perfectly periodic, consistent with the observed wake coherence. In contrast, the signals $\beta = 0.4$ and $\gamma \leqslant 0.5$ have reduced the amplitude in periodicity consistent with behaviour observed in Fig. 3. The only detectable difference between these cases are an increase in frequency and a slight upward shift in the mean of the signal with decreasing gap ratio. These are consistent with the decrease vortex spacing and slight increasing make deflection for smaller gap ratios in Fig. 3.

The change in the amplitude and the degree of regularity of the oscillating lift are consistent with the change to the nature of the wake. For all position ratios $0.25 \leqslant \gamma \leqslant 1$, over $\beta \lesssim 0.3$, the lift coefficient oscillates regularly with a large amplitude consistent with the existence of time periodic vortex shedding from the cylinder (see Fig. 2). At $\gamma = 0.25$ for $\beta = 0.4$, the amplitude reduction and the irregularity of the fluctuating lift correlate with vortex formation much further from the cylinder and reduced regularity of shedding overall.

The respective Fourier spectra of the lift coefficient signals presented in Fig. 5 are plotted in Fig. 6. Consistent with Fig. 5(a), the spectra for $\beta = 0.1$ shown in Fig. 6(a) exhibit a strong harmonic peak for each position ratio considered. This reflects the uniform periodic behaviour observed in the lift coefficient time histories. An modest increase in shedding frequency is found as the cylinder is shifted from the centreline towards the heated duct side-wall.

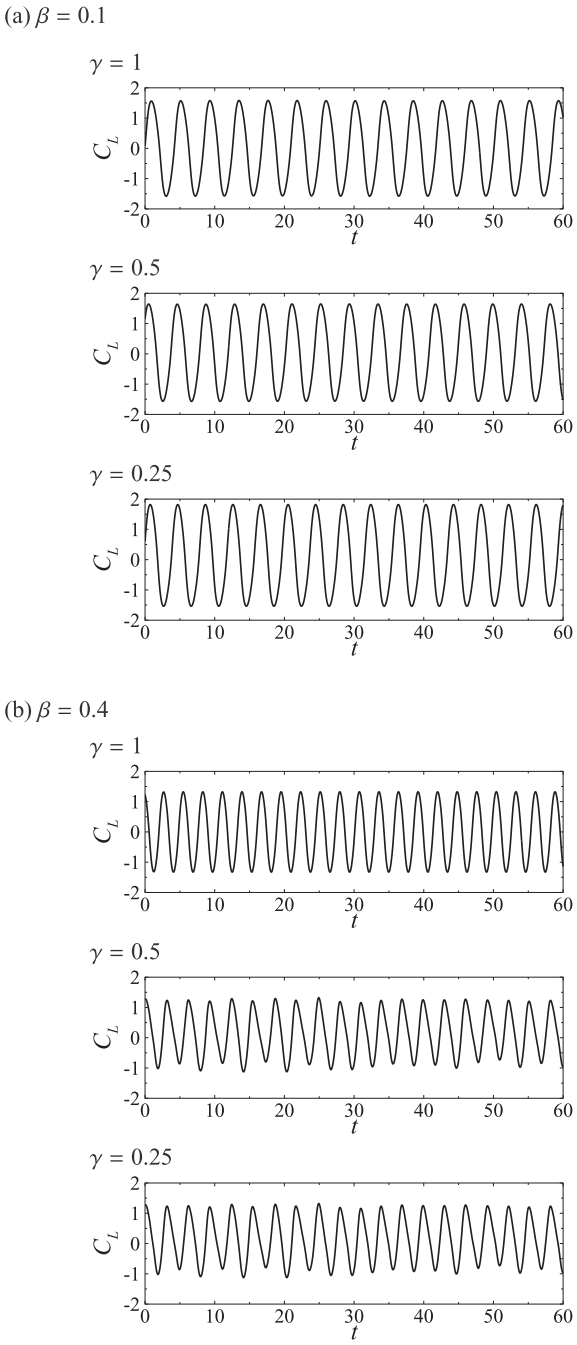

Fig. 5. Time history of lift force coefficient for (a) $\beta = 0.1$ and (b) $\beta = 0.4$ at gap ratios as indicated for $H_d = 100$ and $Re_d = 2000$.

From $\gamma = 1$ down to $\gamma = 0.5$, the increase was approximately 1%, and a further increase of approximately 6% was produced from $\gamma = 0.5$ to $\gamma = 0.25$.

The spectrum for $\beta = 0.4$ and the centreline cylinder position exhibits a strong narrow peak corresponding to highly periodic and uniform vortex shedding. At smaller position ratios, the spectra show an appreciable increase in energy away from the peak, coupled with a widening and reduction in strength of the peak. This reflects the breakdown of uniform periodic lift coefficient time histories seen in Fig. 5(b). A feature absent from the $\beta = 0.1$ Fourier spectra is an *increase* in spectrum energy as frequencies approach zero at $\beta = 0.4$ and $\gamma \leqslant 0.5$. There is approximately a 9% increase in shedding frequency as γ is reduced from 1 to 0.25. The Strouhal frequencies for vortex shedding is approximately 40% higher for $\beta = 0.4$ than for $\beta = 0.1$.

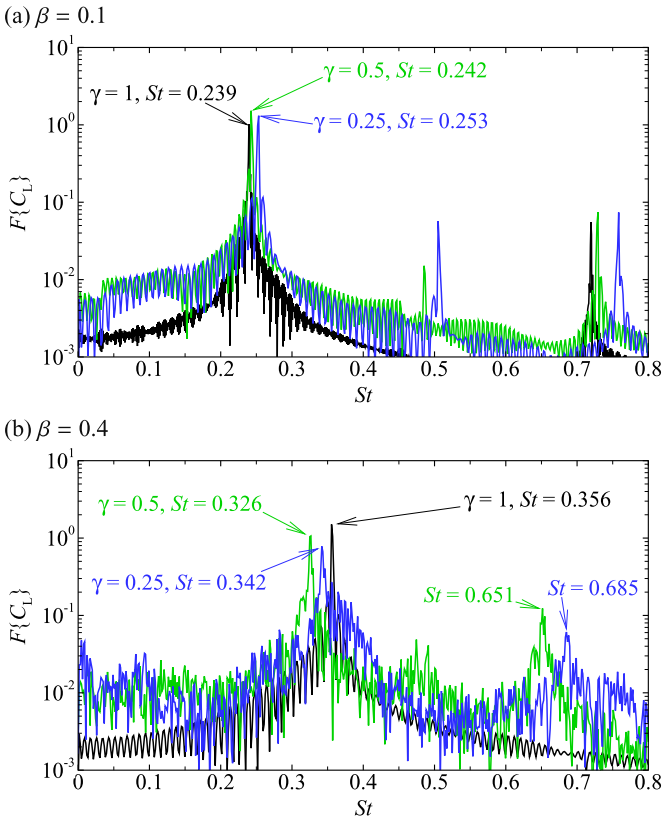

Fig. 6. Fourier spectra of lift coefficient ($F\{C_L\}$) at $Re_d = 2000$ and $H_d = 100$ for blockage ratios (a) $\beta = 0.1$ and (b) 0.4. Position ratios are as indicated in the figures.

4.3. Average Nusselt number of the heated wall

In this section heat transfer from the duct side wall into the flow will be characterized using several parameters. The local Nusselt number along the heated side-wall of the channel is defined as

$$Nu_w(x,t) = \frac{d}{(T_f - T_w)} \left.\frac{\partial T}{\partial y}\right|_{wall}. \tag{13}$$

T_f is the bulk fluid temperature, which is calculated using the velocity and temperature distribution as

$$T_f(x,t) = \frac{\int_{-L}^{L} uT\,\mathrm{d}y}{\int_{-L}^{L} u\,\mathrm{d}y}, \tag{14}$$

where u is the streamwise component of velocity.

A time-averaged Nusselt number for heat transfer through the heated wall of the channel is calculated by first taking the time average of the local Nusselt number ($\overline{Nu}_w$) at each x-station, and then integrating over the length of the heated side-wall, L_{duct}, using

$$Nu = \frac{1}{L_{\mathrm{duct}}} \int_0^{L_{\mathrm{duct}}} \overline{Nu}_w(x)\,\mathrm{d}x. \tag{15}$$

To characterize the effect on the heat transfer due to the addition of a cylinder to the channel, the overall increment of heat transfer is defined as

$$HI = \frac{Nu - Nu_0}{Nu_0} \times 100, \tag{16}$$

where Nu_0 is the time-averaged Nusselt number of the heated region of the same duct without cylinder.

Firstly, the effect of blockage and gap ratio for a fixed Reynolds number is presented, and subsequently the dependence on Re_d is considered.

Fig. 7(a) shows the effect of the offset ratio on the time-averaged Nusselt number from the heated wall at different blockage ratios for $H_d = 100$ and $Re_d = 2000$. It can be noted that for a given blockage ratio, there is a remarkable change in Nu as the position ratio varies from $\gamma = 1$ to 0.25. The change is more pronounced at $\beta = 0.1$ and 0.4. For $\beta = 0.1$, the Nussult number increases substantially as position ratio is decreased from $\gamma = 1$ to 0.25. Similarly, the effect of changing the offset ratio from $\gamma = 1$ to 0.5 on Nu is found to be notable for $\beta = 0.2$. It increases significantly, then decreases gradually with further decrease in position ratio. For $\beta = 0.3$, there is a slight decrease in heat transfer as γ is decreases to 0.5, after that it gradually decreases. As expected, for blockage ratio $\beta = 0.4$, the Nusselt number drops more steeply as offset ratio is further decreased to $\gamma = 0.25$.

The variation of pressure drop caused by the offset of the cylinder for different blockage ratios at $Re_d = 2000$ and $H_d = 100$ is presented in Fig. 7(b). Here, the pressure drop penalty Δp_{cyl} is the difference in pressure drop across identical channels with and without a cylinder. For $\beta \leqslant 0.2$, there is only a small increase in pressure drop as the offset ratio is changed from 1 to 0.5, then it decreases for further increase in γ. However, for $\beta \geqslant 0.3$, the pressure drop increased gradually as it changes from 1 to 0.5. The pressure drop exhibits an increased dependence on offset ratio as the blockage ratio increases, with increasing offset ratio resulting in an increased pressure drop. To demonstrate the significant effect of γ on ΔP_{cyl}, the pressure drop at $\beta = 0.4$ is nearly 6.2 times that at $\beta = 0.1$ as γ changes from 1 to 0.25. For $\beta = 0.3$ and 0.2, it increases by factors 3.4 and 1.9, respectively.

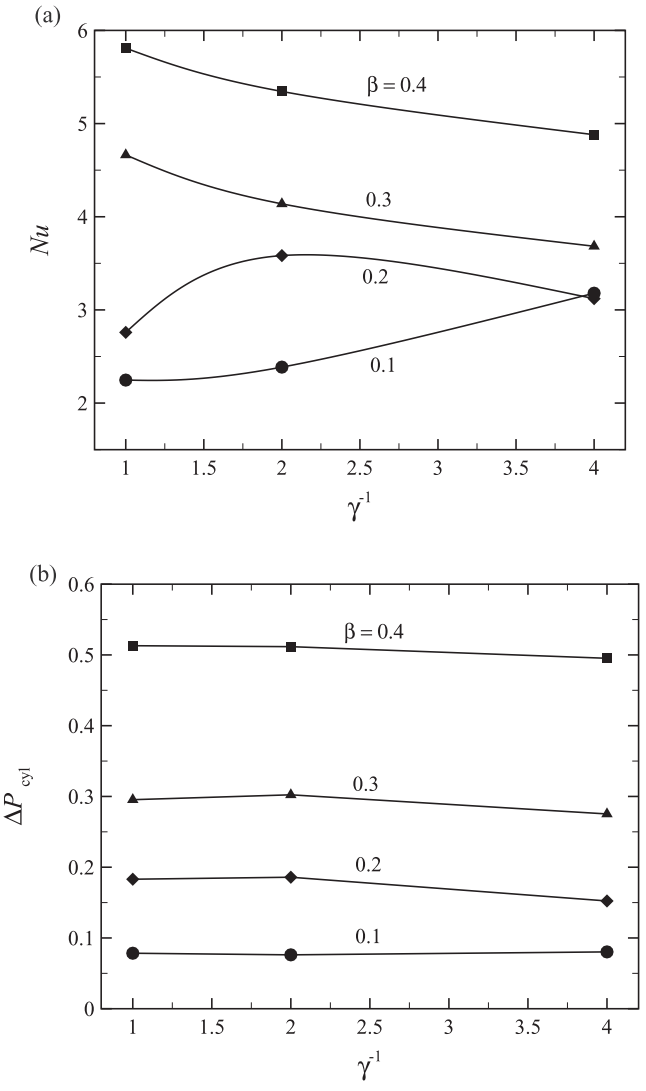

Fig. 7. (a) Time-averaged Nusselt number for heat transfer through the heated wall and (b) pressure drop penalty, each plotted against γ^{-1} at blockage ratios as indicated for $Re_d = 2000$ and $H_d = 100$.

In order to estimate the improvement of the heat transfer achieved by inserting a cylinder within the duct, the percentage increment of the overall heat transfer is calculated using Eq. (16). The percentage increment for $Re_d = 2000$ as γ decreases from 1 to 0.25 for $\beta = 0.1$, 0.2, 0.3 and 0.4 varies between 18–67%, 44–87%, 90–140% and 151–199%, respectively. For $Re_d = 3000$, the increments increases to the respective ranges 23–82%, 50–96%, 114–157% and 189– 228%.

To characterize the quality of heat transfer improvement in this study, both the heat transfer and the pressure drop on the channel are considered. The efficiency index is adopted [46,47] and defined as

$$\eta_{\text{eff}} = \frac{HR}{PR}, \tag{17}$$

where HR and PR are the heat transfer enhancement ratio and pressure penalty ratio, given respectively by

$$HR = \frac{Nu}{Nu_0}, \tag{18}$$

$$PR = \frac{\Delta P}{\Delta P_0}. \tag{19}$$

ΔP is the overall pressure drop across the channel where a circular cylinder is shifted from the channel centerline, and ΔP_0 is the overall pressure drop without a cylinder. The results of percentage heat transfer increments HI, heat transfer enhancement ratio HR, pressure penalty ratio PR and efficiency index η_{eff} for different blockage and offset ratios are listed in Table 2. The results in this table demonstrate that the improvements in heat transfer are much high-

Table 2
Percentage increment of the overall heat transfer and efficiency index obtained by adding the cylinder at different gap ratios from the heated wall. The combinations producing the highest heat transfer increment are highlighted with "*".

β	γ	G/d	HI (%)	HR	PR	η_{eff}	HI_{asym} (%)
$Re_d = 2000$							
0.1	1	4.5	18	1.18	1.05	1.13	
0.1	0.5	2.25	25	1.25	1.05	1.20	6.2
0.1	0.25	1.13	67*	1.67	1.05	1.59*	42
0.2	1	2.0	44	1.44	1.11	1.29	
0.2	0.5	1.0	87*	1.87	1.11	1.68*	29.8
0.2	0.25	0.5	63	1.63	1.09	1.49	13
0.3	1	1.15	140*	2.40	1.17	2.05*	
0.3	0.5	0.58	113	2.13	1.20	1.78	−11.3
0.3	0.25	0.29	90	1.90	1.15	1.65	−21
0.4	1	0.75	199*	2.99	1.30	2.29*	
0.4	0.5	0.38	175	2.75	1.30	2.12	−8
0.4	0.25	0.19	151	2.51	1.29	2.00	−16
$Re_d = 3000$							
0.1	1	4.5	23	1.23	1.08	1.14	
0.1	0.5	2.25	32	1.32	1.11	1.18	7
0.1	0.25	1.13	82*	1.82	1.10	1.65*	48
0.2	1	2.0	50	1.50	1.16	1.30	
0.2	0.5	1.0	96*	1.96	1.25	1.57*	31
0.2	0.25	0.5	67	1.67	1.23	1.36	11.6
0.3	1	1.15	157*	1.23	1.12	1.94*	
0.3	0.5	0.58	133	1.32	1.15	1.72	−9.3
0.3	0.25	0.29	114	1.82	1.11	1.69	−16.5
0.4	1	0.75	228*	2.24	1.16	2.20*	
0.4	0.5	0.38	209	2.07	1.64	2.00	−6
0.4	0.25	0.19	189	1.66	1.13	1.96	−12

er at small blockage ratios, but they are not as great when the cylinder approaches the heated wall (small gap ratio) as it is when the cylinder is located at the mid-plane. It is also noticed from this table that the efficiency index η_{eff} is greater than 1 or nearly 1 for all the cases tested, which indicates that the heat transfer enhancement for this flow is viable.

In addition, to characterize the gain in heat transfer achieved by placing the cylinder near to the heated duct side-wall rather than at the centreline, an offset heat transfer increment is calculated as

$$HI_{\text{asym}} = \frac{Nu_{\text{asym}} - Nu_{\text{sym}}}{Nu_{\text{sym}}} \times 100, \tag{20}$$

where Nu_{asym} and Nu_{sym} represent the time-averaged Nusselt number of the heated surface for the cylinder placed symmetrically or asymmetrically in the duct. The effect of the cylinder on heat transfer improvement can be interpreted from Table 2. When the cylinder approaches the heated wall, higher heat transfer is obtained at small blockage ratio ($\beta \leqslant 0.2$). The reason for this increase may be attributed to the increased velocity of the flow in the vicinity of the heated surface caused by the wake vortices, which leads to an effective mixing between the hot region and cold flow core, leading to a significant increase in heat transfer. The maximum increment in heat transfer is 40.4%, which is obtained at $\gamma = 0.25$ for $\beta = 0.1$ and $Re_d = 2000$ while for $\beta = 0.2$, the maximum heat transfer improvement is occurs at $\gamma = 0.5$, and is 30%. For $Re_d = 3000$, the increments are 48% and 31%, respectively. The table demonstrates that the heat transfer improvement significantly decreases as the cylinder is further from the heated wall of the channel for blockage ratio $\beta \geqslant 0.3$. In fact, the results imply an optimal G/d exists for maximum efficiency. To elucidate this, the variation of efficiency with gap ratio is presented in Fig. 8.

It can be noted from Fig. 8 that the maximum efficiency of heat transfer is achieved near $G/d \approx 1.1$ for $\beta \leqslant 0.3$. These blockage ratios correspond to ducts that are sufficiently wide for the cylinder to be positioned at these gap ratios without crossing the centreline (in this study we have restricted consideration to cylinder positions on the heated side of the duct). The existence of this optimum gap ratio supports earlier discussion in Section 1, as well as observations from Figs. 2 and 3, which show that for $G/d \approx 1$ the wake vortices are cast more closely to the heated wall. As a result, the heat transfer is enhanced significantly due to mixing between

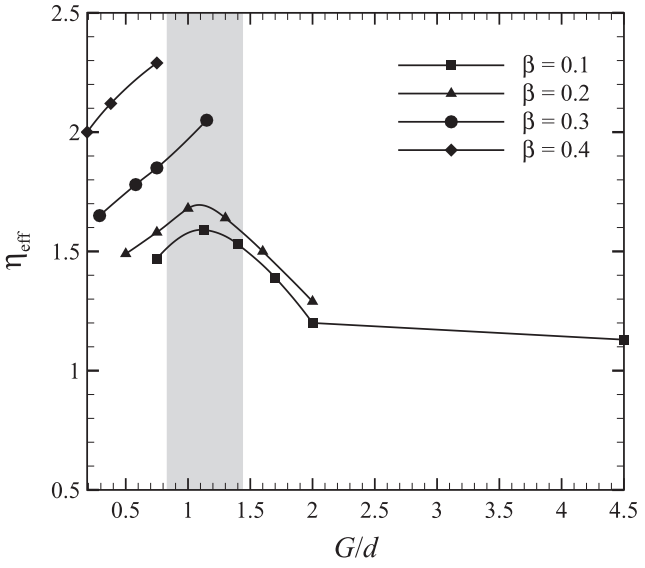

Fig. 8. Variation of the efficiency index with gap ratio G/d at blockage ratios as indicated for $Re_d = 2000$ and $H_d = 100$. The shaded region highlights the zone where η_{eff} is within 95% of its peak value (at $\beta = 0.1$ and 0.2), i.e. $0.83 \leqslant G/d \leqslant 1.4$.

low and high temperature fluids. In Fig. 8 a shaded region captures gap ratios achieving values of η_{eff} that are within 95% of the respecting peak values for each gap ratio. Additionally, comparing G/d and η_{eff} values at $Re_d = 3000$ from Table 2, peak η_{eff} is consistently found at $G/d \approx 1$ in agreement with the $Re_d = 2000$ finding. It should also be noted in the context of the validity of the quasi-two-dimensional model raised in Section 2.1 that the identification of an optimal gap ratio relies on data obtained at smaller blockage ratios, which provide the best adherence to the quasi-two-dimensional assumption under the conditions considered here.

4.4. Reynolds number dependence

Fig. 9 shows the variation of time-averaged Nusselt number Nu of the heated wall with Reynolds number for different blockage and position ratios at $H_d = 100$. It is can be noted that for all Reynolds numbers considered in this study, the variation of the time-averaged Nusselt number shows different behaviour for different ranges of blockage and position ratios, because the flow and the temperature field have different distributions depending on these two parameters. For $\beta = 0.1$ and $\gamma \leqslant 0.5$, there is a slight increase in Nu as the Reynolds number increases. However, it increases significantly at $\gamma = 0.25$. For $\beta = 0.2$, the effect of changing the gap ratio on Nu is negligible for $Re_d \leqslant 1300$. For the remaining range of Reynolds number, there is a considerable increase in Nu as γ varies between 1 and 0.5. However, as the position ratio is further decreased to 0.25, Nu declines substantially for $Re_d \geqslant 2100$. Similarly, for $\beta \geqslant 0.3$, the effect of changing the position ratio on Nu is negligible for the range $Re_d \lesssim 1500$. In fact, for $\beta = 0.3$, there is a gradual decrease in Nu as γ varies between 0.5and 0.25 for $Re_d \geqslant 2000$. The decrease in Nu is more pronounced at $\beta = 0.4$ as γ is increased.

4.5. Streamwise distribution of local Nusselt number

Now the local Nusselt number will be considered both as a function of position x along the heated duct wall, and variation in Reynolds number. Fig. 10 presents the distribution of the local Nusselt number along the heated surface as a function of streamwise coordinate (x) for the maximum and minimum heat transfer enhancement cases plotted in Fig. 8 for $Re_d = 2000$ and $H_d = 100$. This figure shows that for the case that produces maximum heat transfer enhancement, there is a progressive increase in Nu_wover a region extending from the cylinder to a distance approximately $7.5d$ downstream of the cylinder, beyond which it decrease gradually. This region of increasing Nu_w corresponds to a zone of strong interaction between the heated Shercliff layer vorticity and the cylinder wake vortices. For the case producing minimal heat transfer enhancement, Nu_w is seen to decrease monotonically with increasing x, almost indistinguishably from the corresponding curve that would be produced if the cylinder was removed from the channel.

Beyond the trends plotted in Fig. 10, data was also obtained for Reynolds numbers $1000 \leqslant Re_d \leqslant 3000$ at each of $\beta = 0.1$, 0.2, 0.3 and 0.4. Consistently, the effect of increasing Reynolds number was to increase the local Nusselt number. Due to the distance between cylinder and heated Shercliff layer, the $\beta = 0.1$ cases all exhibited the monotonically decreasing Nu_w trends consistent with an absence of wake-Shercliff layer interaction, while for $\beta \geqslant 0.2$, an increasing Reynolds number altered the trends from profiles consistent with no wake-wall interaction to trends consistent with wake-wall interaction. When wake-wall interaction was significant, the location of maximum Nu_w was found to depend irregularly with Reynolds number, blockage ratio and gap ratio, though it always remained within approximately $10d$ downstream of the cylinder. This is consistent with the visualizations provided in Figs. 2–4.

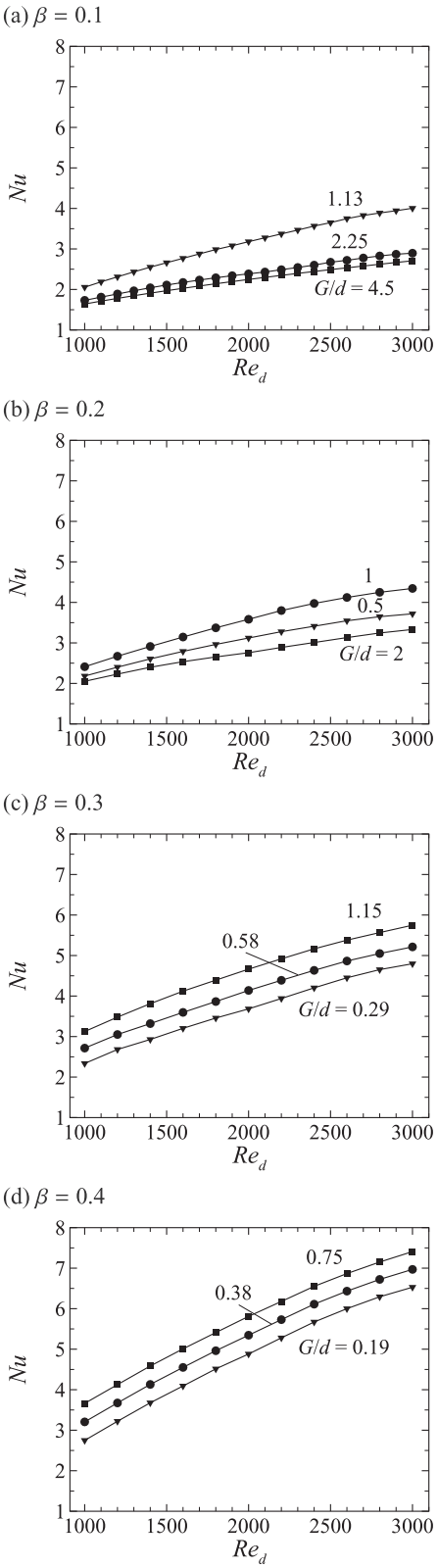

Fig. 9. Time-averaged Nusselt number plotted against Reynolds number at $H_d = 100$ for gap ratios as labelled and blockage ratios (a) $\beta = 0.1$, (b) 0.2, (c) 0.3 and (d) 0.4.

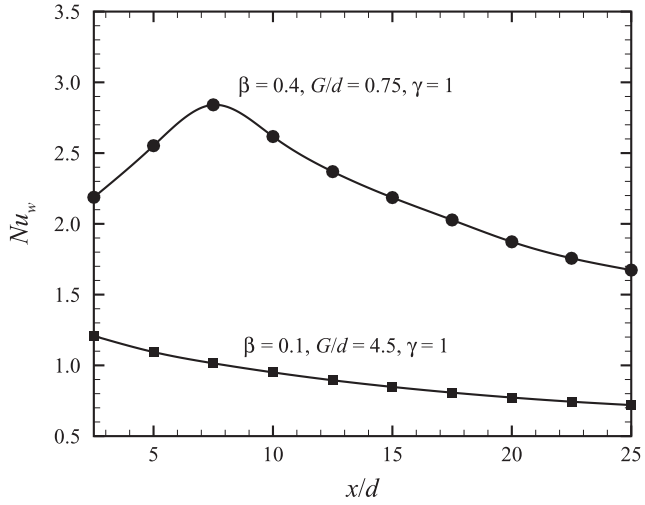

Fig. 10. Time-averaged local Nusselt number plotted against streamwise wall position (relative to the cylinder at $x = 0$) along the heated side wall for $H_d = 100$, and $Re_d = 2000$. The plotted curves correspond to the points with the highest and lowest efficiency index from Fig. 8, $\beta = 0.4$, $G/d = 0.75$) and ($\beta = 0.1$, $G/d = 4.5$), respectively.

5. Conclusions

An investigation has been carried out into the characteristics of MHD flow and heat transfer past a circular cylinder positioned offset from the duct centerline with a strong magnetic field parallel to the cylinder using a spectral-element method. For these conditions, the flow is quasi-two-dimensional and the modified Navier–Stokes equations are solved in a two-dimensional domain. The numerical simulations have been performed over the range of Reynolds number up to 3000, blockage ratio $0.1 \leqslant \beta \leqslant 0.4$, position ratio $0.19 \leqslant \gamma \leqslant 1$ and constant Hartmann number $H_d = 100$. The motivation for this study was inspired by the analysis performed by Hussam et al. [23], which demonstrated that both the heat transfer from the heated wall and the pressure drop penalty increases significantly as the blockage ratio increases.

The results show that the proximity of the cylinder to a wall has a significant influence on the flow and heat transfer characteristics. At $Re_d = 2000$, $\beta = 0.1$ and $0.25 \leqslant \gamma \leqslant 1$, a two-row vortex street is formed with clockwise negative and counter-clockwise positive vortices shed from the top and the bottom shear layers of cylinder maintaining their offsets from the centreline. For $\beta \geqslant 0.2$, the structure of the vortex shedding changes dramatically on further decreasing of gap ratio. The vortex street drifts further away from the wall and convects downstream with long slow decay. For high blockage ratios at $\gamma \geqslant 0.5$, the separating shear layer from the lower side of the cylinder and the boundary layer from the wall effectively merge before combined structures travel further downstream. At the smallest position ratio, the wake vorticity on the upper side of the cylinder elongates as it travels downstream due to the effect of the wall. It is expected that the instability in the wake region should transform from being absolutely unstable at large gaps to convectively unstable at small gaps, which is consistent with the previous findings for non-magnetohydrodynamic bluff body flows.

The characteristics of heat transfer depend strongly on the proximity of the cylinder to the heated wall. This is due to interaction of the boundary layer with the shear layers separating from the cylinder surface. For small blockage ratios, it increases significantly as the position ratio decreases from 1 to 0.25. However, there is a substantial drop in Nusselt number for high blockage ratio. Overall, the enhancement of heat transfer was significantly augmented by 58% through decreasing the position ratio for small blockage ratio (i.e. when the cylinder is close to the wall). In contrast, for $\beta = 0.4$, the maximum heat transfer augmentation was more than twofold, which is found at $\gamma = 1$ (i.e. when the cylinder is placed furthest from the walls) The efficiency index η_{eff} was greater than 1 or nearly 1 for all the cases tested, which

demonstrates that the heat transfer enhancement for this flow is viable. The maximum gain in heat transfer generated by placing the cylinder in the channel near to the wall with that at the centerline was obtained at $\beta = 0.1$ as the cylinder is further approached the heated wall.

The magnitude of the local Nusselt number distribution increases proportionally with Reynolds number and blockage ratio. The position where the each distribution exhibits a maximum value is independent of Reynolds number for small blockage ratios at $\gamma = 0.5$ and 0.25. However, the position moves downstream with increasing Reynolds number for $\beta = 0.4$ at $\gamma = 1$.

Acknowledgments

We thank Professor Alban Pothérat for his suggestion in the embryonic stage of this work to consider the lateral position of the cylinder within the channel in terms of its distance to the heated wall relative to the cylinder diameter.

This work is supported by the Australian Research Council through Discovery Grant DP120100153, and high-performance computing time allocations from the National Computational Infrastructure (NCI) Merit Allocation Scheme and the VLSCI Resource Allocation Scheme. NCI is supported by the Australian Commonwealth Government.

References

[1] J. Sommeria, R. Moreau, Why, how, and when, MHD turbulence becomes two-dimensional, J.Fluid Mech. 118 (1982) 507–518.
[2] J. Moreau, R. Sommeria, Electrically driven vortices in a strong magnetic field, J. Fluid Mech. 189 (1988) 553–569.
[3] A. Pothérat, J. Sommeria, R. Moreau, An effective two-dimensional model for MHD flows with transverse magnetic field, J. Fluid Mech. 424 (2000) 75–100.
[4] I.R. Kirillov, C.B. Reed, L. Barleon, K. Miyazaki, Present understanding of MHD and heat transfer phenomena for liquid metal blankets, Fusion Eng. Des. 27 (1995) 553–569.
[5] L. Bühler, Instabilities in quasi-two-dimensional magnetohydrodynamic flows, J. Fluid Mech. 326 (1996) 125–150.
[6] S. Smolentsev, N. Vetcha, R. Moreau, Study of instabilities and quasi-two-dimensional turbulence in volumetrically heated magnetohydrodynamic flows in a vertical rectangular duct, Phys. Fluids 24 (2012) 024101.
[7] N. Vetcha, S. Smolentsev, M.A. Abdou, R. Moreau, Study of instabilities and transitions for a family of quasi-two-dimensional magnetohydrodynamic flows based on a parametrical model, Phys. Fluids 25 (2013) 024102.
[8] Y.B. Kolesnikov, A.B. Tsinober, Two-dimensional turbulent flow behind a circular cylinder, Magn. Gidrodin 8 (1972) 300–307.
[9] S.Y. Smolentsev, D.A. Dazhi, The effect of a conducting inclusion on the heat transfer in a fully developed MHD flow in a rectangular channel, Magnetohydrodynamics 32 (1996) 331–335.
[10] S. Cuevas, S. Smolentsev, M.A. Abdou, On the flow past a magnetic obstacle, J. Fluid Mech. 553 (2006) 227–252.
[11] S. Cuevas, S. Smolentsev, M.A. Abdou, Vorticity generation in creeping flow past a magnetic obstacle, Phys. Rev. E 74 (2006) 056301.
[12] S. Smolentsev, R. Moreau, L. Bühler, C. Mistrangelo, MHD thermofluid issues of liquid-metal blankets: phenomena and advances, Fusion Eng. Des. 85 (2010) 1196–1205.
[13] J.C.R. Hunt, K. Stewartson, Magnetohydrodynamic flow in rectangular ducts. II, J. Fluid Mech. 23 (1965) 563–581.
[14] M. Frank, L. Barleon, U. Müller, Visual analysis of two-dimensional magnetohydrodynamics, Phys. Fluids 13 (2001) 2287–2295.
[15] A. Pothérat, J. Sommeria, R. Moreau, Numerical simulations of an effective two-dimensional model for flows with a transverse magnetic field, J. Fluid Mech. 534 (2005) 115–143.
[16] A. Pothérat, Quasi-two-dimensional perturbations in duct flows under transverse magnetic field, Phys. Fluids 19 (2007) 074104.
[17] D. Krasnov, O. Zikanov, T. Boeck, Numerical study of magnetohydrodynamic duct flow at high Reynolds and Hartmann numbers, J. Fluid Mech. 704 (2012) 421–446.
[18] H. Kobayashi, Large eddy simulation of magnetohydrodynamic turbulent duct flows, Phys. Fluids 20 (2008) 015102.
[19] L.G. Kit, S.V. Turuntaev, A.B. Tsinober, Investigation with a conduction anemometer of the effect of magnetic field on disturbances in the wake of a cylinder, Magn. Gidrodin. 6 (1970) 35–40.
[20] D.D. Papailiou, Magneto-fluid-mechanic turbulent vortex streets, Progr. Astronaut. Aero 100 (1985) 152–173.
[21] B. Muck, C. Gunther, U. Müller, L. Bühler, Three-dimensional MHD flows in rectangular ducts with internal obstacles, J. Fluid Mech. 418 (2000) 265–295.
[22] V. Dousset, A. Pothérat, Numerical simulations of a cylinder wake under a strong axial magnetic field, Phys. Fluids 20 (2008) 017104.
[23] W.K. Hussam, M.C. Thompson, G.J. Sheard, Dynamics and heat transfer in a quasi-two-dimensional MHD flow past a circular cylinder in a duct at high Hartmann number, Int. J. Heat Mass Transfer 54 (2011) 1091–1100.
[24] L. Barleon, U. Burr, R. Stieglitz, M. Frank, Heat transfer of a MHD flow in a rectangular duct, in: A. Alemany, P. Marty, J.P. Thibault (Eds.), Transfer Phenomena in Magnetohydrodynamic and Electroconducting Flows: Selected papers of the PAMIR Conference held in Aussois, France, 22–26 September, 1997, Fluid Mechanics and its Applications, vol. 51, Kluwer Academic Publishers, Aussois, France, 1997, ISBN 978-3-642-03085-7, pp. 305–309.
[25] W.K. Hussam, M.C. Thompson, G.J. Sheard, Optimal transient disturbances behind a circular cylinder in a quasi-two-dimensional magnetohydrodynamic duct flow, Phys. Fluids 24 (2012) 024150.
[26] W.K. Hussam, M.C. Thompson, G.J. Sheard, Enhancing heat transfer in a high Hartmann number magnetohydrodynamic channel flow via torsional oscillation of a cylindrical obstacle, Phys. Fluids 24 (2012) 113601.
[27] P.W. Bearman, M.M. Zdravkovich, Flow around a circular cylinder near a plane boundary, J. Fluid Mech. 89 (1978) 33–47.
[28] G. Bosch, M. Kappler, W. Rodi, Experiments on the flow past a square cylinder placed near a wall, Exp. Thermal Flow Sci. 13 (1996) 292–305.
[29] C. Lei, L. Cheng, K. Kavanagh, Re-examination of the effect of a plane boundary on force and vortex shedding of a circular cylinder, J. Wimd Eng. Indust. Aerodyn. 80 (1999) 263–286.
[30] C. Lei, L. Cheng, S.W. Armfield, K. Kavanagh, Vortex shedding suppression for flow over a circular cylinder near a plane boundary, Ocean Eng. 27 (2000) 1109–1127.
[31] S.J. Price, D. Sumner, J.G. Smith, K. Leong, M.P. Païdoussis, Flow visualization around a circular cylinder near to a plane wall, J. Fluids Struct. 16 (2002) 175–191.
[32] S. Bailey, R. Martinuzzi, G. Kopp, The effects of wall proximity on vortex shedding from a square cylinder: three-dimensional effects, Phys. Fluids 14 (2002) 4160–4177.
[33] S. Mettu, N. Verma, R. Chhabra, Momentum and heat transfer from an asymmetrically confined circular cylinder in a plane channel, Heat Mass Transfer 42 (2006) 1037–1048.
[34] U. Burr, L. Barleon, U. Müller, A. Tsinober, Turbulent transport of momentum and heat in magnetohydrodynamic rectangular duct flow with strong sidewall jets, J. Fluid Mech. 406 (2000) 247–279.
[35] L. Barleon, U. Burr, K.-J. Mack, R. Stieglitz, Heat transfer in liquid metal cooled fusion blankets, Fusion Eng. Des. 51–52 (2000) 723–733.
[36] G.J. Sheard, M.P. King, The influence of height ratio on Rayleigh-number scaling and stability of horizontal convection, Appl. Math. Modell. 35 (2011) 1647–1655.
[37] M.A. Hossain, Viscous and Joule heating effects on MHD-free convection flow with variable plate temperature, Int. J. Heat Mass Transfer 35 (1992) 3485–3487.
[38] H.S. Yoon, H.H. Chun, M.Y. Ha, H.G. Lee, A numerical study on the fluid flow and heat transfer around a circular cylinder in an aligned magnetic field, Int. J. Heat Mass Transfer 47 (2004) 4075–4087.
[39] R.J. Lingwood, T. Alboussiere, On the stability of the Hartmann layer, Phys. Fluids 11 (1999) 2058–2068.
[40] G. Authié, T. Tagawa, R. Moreau, Buoyant flow in long vertical enclosures in the presence of a strong horizontal magnetic field. Part 2: Finite enclosures, Eur. J. Mech. B/Fluids 22 (2003) 203–220.
[41] N. Kanaris, X. Albets, D. Grigoriadis, S. Kassinos, Three-dimensional numerical simulations of magnetohydrodynamic flow around a confined circular cylinder under low, moderate, and strong magnetic fields, Phys. Fluids 25 (2013) 074102.
[42] G.E. Karniadakis, M. Israeli, S.A. Orszag, High-order splitting methods for the incompressible Navier–Stokes equations, J. Comput. Phys. 97 (1991) 414–443.
[43] G.E. Karniadakis, S.J. Sherwin, Spectral/hp Element Methods for Computational Fluid Dynamics, Oxford University Press, 2005.
[44] G.J. Sheard, T. Leweke, M.C. Thompson, K. Hourigan, Flow around an impulsively arrested circular cylinder, Phys. Fluids 19 (2007) 083601.
[45] G.J. Sheard, Wake stability features behind a square cylinder: focus on small incidence angles, J. Fluids Struct. 27 (2011) 734–742.
[46] Y.-Y. Tsui, S.-W. Leu, C.-C. Lin, P.-W. Wu, Heat transfer enhancement by multilobe vortex generators: effects of lobe parameters, Numer. Heat Transfer 37 (2000) 653–672.
[47] S.-J. Yang, Numerical study of heat transfer enhancement in a channel flow using an oscillating vortex generator, Heat Mass Transfer 39 (2003) 257–265.